Preprints of the 21st IFAC World Congress (Virtual)
Berlin, Germany, July 12-17, 2020

Model-based temperature offset compensation for additive manufacturing by directed energy deposition ⋆

David Dillkötter * **Johann Stoppok** * **Magnus Thiele** *
Cemal Esen * **Martin Mönnigmann** *

* *Department of Mechanical Engineering, Ruhr-Universität Bochum, 44801 Bochum, Germany (e-mail: david.dillkoetter@rub.de, johann.stoppok@rub.de, thiele@lat.rub.de, esen@lat.rub.de and martin.moennigmann@rub.de).*

Abstract: Laser based directed energy deposition (DED), also known as laser metal deposition or laser cladding, is an additive manufacturing technology for building 3D freeform parts. Reliable temperature measurements are of obvious interest and importance for the control of these processes. We propose a model-based method for the correction of temperature measurements from an imperfectly aligned sensor, which is a pyrometer in our process. We show that the proposed method can improve the reliability of the pyrometer-based temperature measurements even if the pyrometer is carefully aligned and calibrated according to industrial standards. We apply the proposed method to a powder-based directed energy deposition process. Due to its simplicity, the proposed method can easily be adapted to other additive manufacturing process types.

Keywords: additive manufacturing, directed energy deposition, process control, metal processing, manufacturing plant control

1. INTRODUCTION

Laser-based directed energy deposition (DED) belongs to the family of additive manufacturing processes (Gibson et al., 2015). The process type treated here is characterized by a laser energy source and a powder feeding system that adds material through a nozzle onto the substrate (see Figure 1). As in many other additive processes, 3D freeform parts can be created using this technique by moving the nozzle according to a precomputed path.

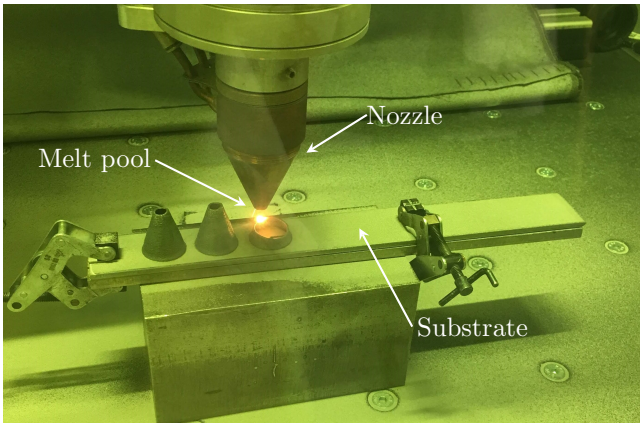

Fig. 1. Laboratory laser based DED machine

⋆ This work was supported by the German Federal Ministry of Education and Research under grant 13N14305 (project "iTSELF").

Because temperature gradients are typically very large (room temperature to more than 2000K in the printed part, see Figure 5) and because materials like steel and aluminum have high thermal conductivities, temperature control is challenging in directed energy deposition processes. Most importantly, reliable methods for monitoring and controlling the melt pool temperature are required.

Devesse et al. (2017) present a controller for the melt pool temperature that is based on a thermal camera. The measurement of the temperature distribution is used to control the melt pool width with a combination of linear state feedback and PI control in this case. Song and Mazumder (2010) use a pyrometer to monitor and control temperature. The proposed controller is based on a experimentally identified state-space model. Wang et al. (2017) develop a physics-based model for the melt pool height and temperature and propose a MIMO controller for these two variables.

We present a model-based method for increasing the reliability of temperature measurements. The proposed approach is essentially based on determining the offset of the intended to the actual point or area of the temperature measurement. The melt pool temperature can be characterized by elliptical isotherms (see, e.g., Devesse et al. (2014)). Due to the relative motion of the DED process head to the substrate, these ellipses are not point-symmetric with respect to the heat source (the laser spot or focus), but the temperature gradient is steeper in the direction of the head velocity (see Section 2 for illustrations). If the pyrometer is attached to the head but its

measurement area A_p is not perfectly aligned with the laser focus, the location A_p with respect to the isotherms will be a function of the head velocity. The pyrometer will, for example, measure an erroneously low temperature if A_p happens to be located in front of the laser focus in the direction of the current head velocity. Conversely, it will measure an erroneously high temperature if the head velocity is reversed. The error due to the misalignment obviously is a function of the head velocity. We note that a laterally mounted pyrometer also results in a strongly directional dependent measurement (Gibson et al., 2015).

We propose a model-based calculation and correction of the misalignment of the temperature measurement area. We apply this method to a DED process that is equipped with a pyrometer. The proposed approach is able to reduce the measurement error and its calibration can be automated. We show that the computational effort can be reduced to allow for an implementation on an embedded device.

The proposed method is not limited to DED processes and can easily be extended to other process types containing a moving point heat source.

In Section 2 we introduce a model of the melt pool based on the heat conduction equation. Its solution for a point heat source, the Rosenthal equation, predicts the directional dependency of a misaligned pyrometer. We use this model to derive a simple procedure for compensating the misalignment in Section 3. Sections 4 and 5 report results obtained for an actual DED process and a conclusion, respectively.

2. PROCESS AND DEVICE MODEL

Two Cartesian coordinate systems are required throughout the paper. They are illustrated in Fig. 2. The axis labeled x, y and z span the *machine coordinate system* that is fixed with respect to the laboratory. The second system with axes labeled ξ, η, ζ, which we refer to as the *nozzle coordinate system*, is centered at the laser focus with the ξ-axis pointing in the negative direction of the velocity U of the nozzle and laser, where U is measured in the machine coordinate system. The (x, y)- and (ξ, η)-planes are coplanar and material is built up in the direction orthogonal to these planes in positive (z, ζ)-direction. Let ϕ refer to the angle between the x- and ξ- axes (see Figure 2). We assume the laser and powder nozzle can be moved linearly along all three axes. Note that the nozzle coordinate system rotates and ϕ changes whenever U changes direction. In contrast, the machine head with the nozzle (and the pyrometer attached to it) do not rotate, but they are moved linearly along the x-, y- and z-axis only. Only velocities $U = (U_1, U_2, 0)^T$ in the plane are required in the present paper.

The velocity U depends on ϕ according to

$$U(\phi) = \begin{pmatrix} \cos(\phi) \\ \sin(\phi) \end{pmatrix} \|U\|_2.$$

We state the inverse $\phi(U)$ for later use. It reads

$$\phi(U) = \arctan_2(U_1, U_2) \tag{1}$$

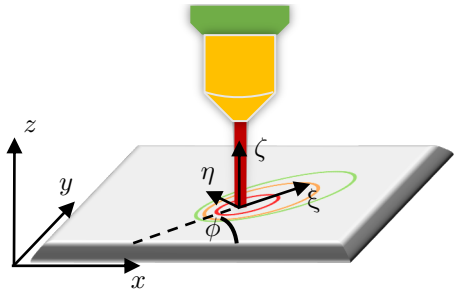

Fig. 2. Machine coordinate system (x, y, z) and nozzle coordinate system (ξ, η, ζ).

2.1 Energy deposition process model

We assume the laser deposits energy into a semi-infinite $(z \leq 0)$ work piece with a surface coplanar to the (x, y)-plane. If the laser heat source and the work piece move with a constant relative velocity $\|U\|_2$, the temperature distribution in the work piece can be modeled with the heat conduction equation (see, e.g., Dowden (2001, Chapter 4.2))

$$\frac{\partial T}{\partial t} = \alpha \left(\frac{\partial^2 T}{\partial \xi^2} + \frac{\partial^2 T}{\partial \eta^2} + \frac{\partial^2 T}{\partial \zeta^2} \right) - \|U\|_2 \frac{\partial T}{\partial \xi}, \tag{2}$$

with thermal diffusivity α, which is assumed to be independent of temperature, and where the material is assumed to be isotropic and homogeneous. The steady state solution of (2) for boundary conditions that model a point source and for constant temperature initial condition is given by the Rosenthal equation (Rosenthal, 1946)

$$T(\xi, \eta; U, P) = T_0 + \frac{A_b P}{2\pi k r} \exp\left(\frac{(\xi - r)\|U\|_2}{2\alpha} \right) \tag{3}$$

where $r = \sqrt{\xi^2 + \eta^2}$, P is the power of the laser, A_b is the absorption coefficient, k is the thermal conductivity and $L = 2\alpha / \|U\|_2$. Note that (3) describes the temperature distribution in the nozzle coordinate system. Elliptical isotherms result, which are sketched in Figure 3.

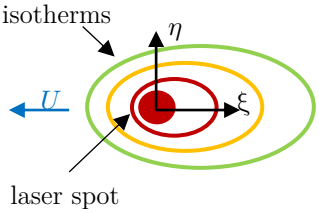

Fig. 3. Sketch of the isotherms that result for the Rosenthal equation (3)

2.2 Measurement device model

Temperatures are determined with a pyrometer. The typical setup used in laser-based directed energy deposition devices is sketched in Figure 4. The pyrometer integrates the radiation emitted by an area A_p and determines the corresponding black body temperature T_p based on the Stefan-Boltzmann law according to

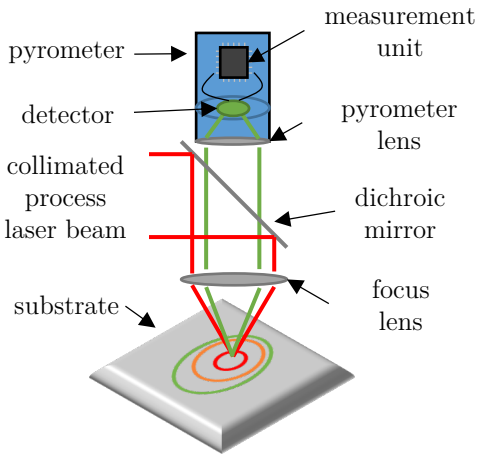

Fig. 4. Pyrometer geometry. Ellipses are the same sketched isotherms as in Fig. 3.

$$P_{\text{rad}} = \sigma \int_{A_\text{p}} \bar{T}^4(\xi,\eta;U)dA \tag{4a}$$

$$= \sigma T_\text{p}^4 \int_{A_\text{p}} dA = \sigma T_\text{p}^4 A_\text{p} \tag{4b}$$

with Stefan-Boltzmann constant σ, and where A_p denotes both the surface and the surface area by a slight abuse of notation. The temperature $\bar{T}$ in (4a) is equal to (3) up to a saturation introduced by the pyrometer, i.e.,

$$\bar{T}(\xi,\eta;U,P) = \min\left(T_{\text{p,max}}, T(\xi,\eta;U,P) \text{ from (3)}\right) \tag{5}$$

where $T_{\text{p,max}} = 2573\text{K}$ in Section 4 . Assuming the pyrometer has a limiting circular aperture, the area A_p is a circle (in spite of a possibly rectangular sensor) with radius r_{pyro}, i.e.,

$$A_\text{p} = \pi r_{\text{pyro}}^2. \tag{6}$$

While the saturation temperature $T_{\text{p,max}}$ is typically known, the limiting aperture and thus the radius r_{pyro} are typically not known. The optical properties of the pyrometer and all other optical components involved would have to be accounted for in order to determine r_{pyro} by reverse engineering. We determine A_p and r_{pyro} with a parameter estimation instead (Section 3.1).

We assume the laser wavelength of the laser and wavelength interval measured by the pyrometer to be far enough apart. All parameter values are given in the appendix.

2.3 Pyrometer offset

Unfortunately, the area A_p captured by a pyrometer cannot be expected to be centered at the origin of the nozzle coordinate system. Manufacturing tolerances, maintenance or incorrect use of the machine result in an offset that must be compensated for, if the temperature signal is to be used for quality or feedback control (see Fig. 5a for an illustration).

We assume an offset exists that is constant in the machine coordinate system. This assumption is valid if the offset changes only slowly over the lifetime of the manufacturing device. Figure 5 illustrates that an offset that is constant in the machine coordinate system is a function of the nozzle

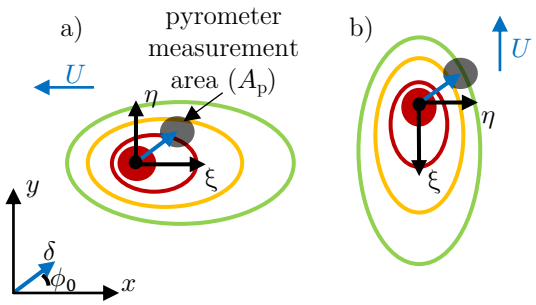

Fig. 5. Directional dependence of the pyrometer measurement error. The offset (blue vector) of A_p (grey disk) with respect to the laser focus (red disk) does not depend on U. The orientation of the elliptical isotherms, in contrast, does depend on U. The measurement error of the pyrometer therefore depends on U.

velocity U in the nozzle coordinate system. This implies that the apparent temperature measured by the pyrometer must be compensated for as a function of U. Let $\bar{\delta}$ and δ refer to the offset in the nozzle and machine coordinate systems, respectively. Then

$$\bar{\delta}(U) = \begin{pmatrix}\cos(\phi_0 - \phi(U))\\ \sin(\phi_0 - \phi(U))\end{pmatrix} \|\delta\|_2, \tag{7}$$

where $\phi(U)$ is as introduced in (1) and $\|\bar{\delta}\|_2 = \|\delta\|_2$. With this offset, the area actually captured by the pyrometer is given by

$$A_\text{p} = \left\{ \begin{pmatrix}\bar{\delta}_1 + \rho\cos(\varphi)\\ \bar{\delta}_2 + \rho\sin(\varphi)\end{pmatrix} \,\middle|\, \rho \in [0, r_{\text{pyro}}],\ \varphi \in [0, 2\pi) \right\}$$

and (4a) yields

$$P_{\text{rad}}/\sigma = \int_0^{r_{\text{pyro}}} \int_0^{2\pi} \bar{T}^4\left(\bar{\delta}_1 + \rho\cos(\varphi), \bar{\delta}_2 + \rho\sin(\varphi); U, P\right) \rho d\rho d\varphi \tag{8}$$

where $\bar{T}$ is as in (5). With (4b) and (6) this yields

$$T_\text{p} = \left(\frac{P_{\text{rad}}/\sigma}{\pi r_{\text{pyro}}^2}\right)^{1/4} \tag{9}$$

T_p depends on the clipped temperature $\bar{T}$ from (5) and thus the actual temperature field $T(\xi,\eta;U,P)$ described by (3), on the known parameter U also via (7), and on the unknown parameters ϕ_0, $\|\delta\|_2$ and r_{pyro} via (7) and (9), respectively. This is summarized for later use by denoting the left hand side in (9) by

$$T_\text{p}(\bar{T}(\cdot), U, P; \phi_0, \|\delta\|_2, r_{\text{pyro}}), \tag{10}$$

where $\bar{T}(\cdot)$ is short for $\bar{T}(\xi,\eta;U,P)$ defined in (5) and the semicolon separates known from unknown quantities.

We illustrate (8)-(10) with Figure 6. Figure 6 shows T_p as a function of the offset distance $\|\delta\|_2$ and offset angle ϕ of the measurement area (see Figure 5 for the meaning of $\|\delta\|_2$ and ϕ):

- If no offset exists ($\|\delta\|_2 = 0$, Figure 6a), the temperature T_p measured by the pyrometer does not depend on the direction of U. The temperature is a function of $\|U\|_2$ but it is independent of ϕ as predicted by (3).
- If there exists an offset ($\|\delta\|_2 > 0$, Figures 6b and 6c), the pyrometer does not measure the correct temperature, and the error is a function of the direction

of motion of the process head or, more specifically, of $\phi - \phi_0$. The error gets larger as $\|U\|_2$ increases (compare Figures 6b and 6c).

The error amounts to up to 6% for the process parameters that were used to obtain the data shown in Figure 5, which corresponds to an absolute error of more than 120K. The error increases to over 10% for the device used here if the laser power is increased (data not shown).

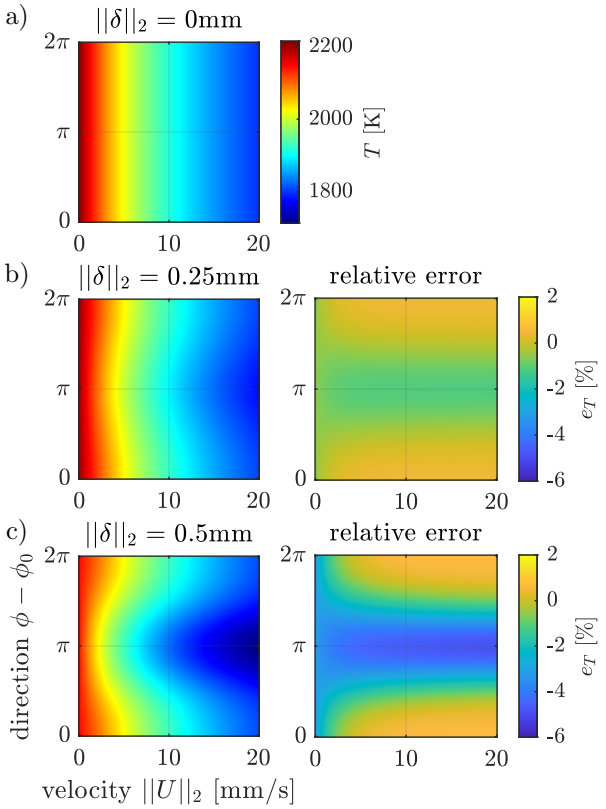

Fig. 6. Left column: T_p as a function of $\phi - \phi_0$ and $\|U\|_2$ for $P = 250$W and the parameters given in the appendix. Right column: Relative error with respect to the temperatures from a.

3. OFFSET IDENTIFICATION AND CORRECTION

We determine the unknown parameters in (10) with an automated procedure in Section 3.1. The resulting model can then be used to compensate the pyrometer offset. This is discussed in Section 3.2.

3.1 Automated calibration

The unknown parameters r_{pyro}, ϕ_0 and $\|\delta\|_2$ in (10) can be determined by solving the nonlinear least-squares optimization problem

$$\min_{\|\delta\|_2, \phi_0, r_{\text{pyro}}} \sum_{k=1}^{K} \left(T_{\text{exp}}^{(k)} - T_{\text{p}}(\bar{T}(\cdot), U^{(k)}; \phi_0, \|\delta\|_2, r_{\text{pyro}}) \right)^2 \tag{11}$$

where $T_{\text{exp}}^{(k)}$, $k = 1, \ldots, K$ refer to K temperatures measured with the pyrometer for velocities $U^{(k)}$, $k = 1, \ldots, K$ with constant magnitude $\|U^{(k)}\|_2 = \|U\|_2$ but varying direction.

We obtain the required data $T_{\text{exp}}^{(k)}$, $U^{(k)}$, $k = 1, \ldots, K$ from measurements taken during an automated calibration run along a circular path on a solid substrate. Sample data from multiple calibration runs is shown in Figure 7. The directional dependency of the measurement can clearly be seen in the graph. For example, the temperature exceeds 2000K around $\phi = 3\pi/4$, while it stays well below this temperature around $\phi = 7\pi/4$. Note that this results in spite of a careful manual adjustment of the pyrometer with a pilot laser.

We carried out all nonlinear least squares estimations (11) with $N = 36$ samples, where this number is arbitrary and was merely chosen because it proved to be sufficiently large. The diameter of the calibration circle was 10mm. The laser power was set to 250W, which is equal to the mean admissible power of the laser of our DED device. The data shown in Figure 7 resulted in a set of offset parameters $\phi_0 = 4.1$, $\|\delta\|_2 = 0.28mm$ and $r_{\text{pyro}} = 0.91mm$. Figure 8 indicates the nonlinear parameter estimation worked adequately. A more quantitative discussion is given below.

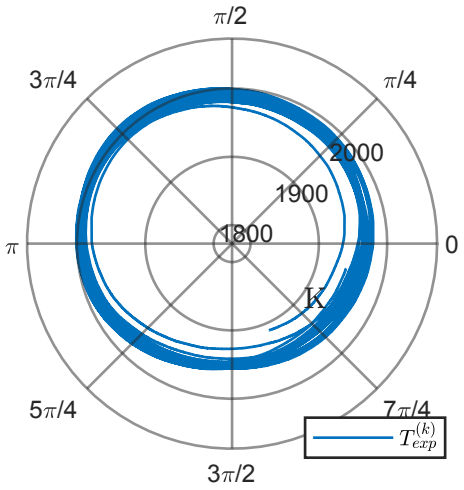

Fig. 7. Sample data for (11) measured along a circular path. The plot shows the temperature measured with the pyrometer as a function of ϕ.

3.2 Digital correction

It is the purpose of the pyrometer to provide a temperature at a defined point (ξ_0, η_0) in the nozzle coordinate system, where this point must not depend on the nozzle velocity U. For example, (ξ_0, η_0) may be chosen to be a point at which the melting temperature T_m is reached for the nominal process parameters, i.e., $\bar{T}(\xi_0, \eta_0; U_0, P_0) = T_m$, for the nominal nozzle velocity U_0 and laser power P_0. The temperature measured at (ξ_0, η_0) may then be used to control the melt pool size by using P as the manipulated variable, for example.

Once the offset of the pyrometer has been determined with the approach described in Section 3.1, all parameters of T_{p} in (10) are known. Evaluating T_{p} at the point of interest (ξ_0, η_0) therefore yields the desired temperature. In

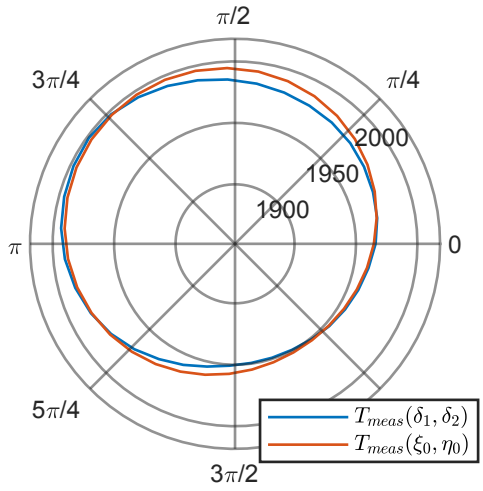

Fig. 8. Comparison of measured temperatures (blue) and temperatures predicted with (10) and estimated parameters (red). A subset of the data from Figure 7 is shown only for better visibility.

the real process, however, disturbances and plant-model-mismatch will obviously cause the predicted temperature to deviate from the actual one.

Instead of merely evaluating T_p after adjusting the model with data from a calibration run, we intend to use the pyrometer in real-time during the actual DED process. This implies the following steps: (i) Measuring the temperature $T_\mathrm{meas}(\delta_1, \delta_2)$ with the pyrometer at the true offset δ, where δ is determined as described in Section 3.1; (ii) evaluating $T_\mathrm{p}(\xi, \eta)$ at $(\xi, \eta) = (\delta_1, \delta_2)$ and the current U, P and parameters of the pyrometer offset that resulted from the calibration described in Section 3.1; (iii) determining the approximate temperature at the point of interest (ξ_0, η_0) from

$$T_\mathrm{meas}(\xi_0, \eta_0) = \frac{T_\mathrm{meas}(\delta_1, \delta_2)}{T_p(\delta_1, \delta_2)} T_p(\xi_0, \eta_0). \tag{12}$$

Equation (12), or equivalently,

$$\frac{T_\mathrm{meas}(\xi_0, \eta_0)}{T_p(\xi_0, \eta_0)} = \frac{T_\mathrm{meas}(\delta_1, \delta_2)}{T_p(\delta_1, \delta_2)}$$

is obviously a linear approximation. We will show that it is sufficiently precise in Section 4.

Note that steps (ii) and (iii) require to numerically evaluate the integral (8). Since this step is too computational expensive for an online evaluation in our laboratory setup, we record the results of steps (i)–(iii) solutions in a look-up table, which is described in Section 4. The look-up table spans an equidistant grid in the parameters direction ϕ, velocity $\|U\|_2$ and laser power P. Because of the equidistant grid, no computationally expensive point location problems need to be solved. A trilinear interpolation is carried out for the eight nearest neighbors of the value $(\phi, \|U\|_2, P)$ of interest (see, e.g., Bai and Wang (2010)). The parameter intervals and numbers of grid points used for our particular laboratory setup are stated in Section 4.

4. EXPERIMENTAL VALIDATION

We applied the proposed compensation method to a laser based DED machine (OR Laser Evo Cube). The maximum power of the laser source (IPG YLM-400), which is connected to the machine head by an optical fiber, amounts to $P = 450$W. The head, which can be moved with velocities of up to 20mm/s, is equipped with a coaxial nozzle and a pyrometer (Metis M3 H322) with a sampling rate of up to 25kHz. The substrate is a solid stainless steel plate (type 1.4301). We note for completeness that the powder material is stainless steel (316l); all data reported here were generated for zero powder flow. We use a laser power of $P = 250$W and $\|U\|_2 = 10$mm/s in our tests. The absorption coefficient was determined in earlier experiments with the same device and set to $A_b = 0.625$.

We adjusted the pyrometer manually with a pilot laser according to the manufacturer's instructions. Subsequently, we carried out the automated calibration as proposed in Section 3.1. Although the pyrometer was aligned carefully, the automated calibration detected an offset of $\phi_0 = 4.1$, $\|\delta\|_2 = 0.28$mm and $r_0 = 0.91$mm. Note that $\|\delta\|_2 = 0.28$mm is approximately as large as the offset used in the illustration shown in Figure 7b (0.25mm). Therefore, we expect a similar error as in Figure 7, i.e., about ±30K, for a melt pool temperature of about 2000K. We note for completeness that the automated calibration determined the apparent radius of the pyrometer to be $r_0 = 0.91$mm.

To implement the digital correction proposed in Section 3.2, we constructed a look-up table with the dimensions $N_\phi = 30, N_{\|U\|_2} = 30, N_P = 30$, which requires 108kB of memory. The look-up table covers the intervals $\phi \in [0, 2\pi]$, $\|U\|_2 \in [0, 20]$mm/s and $P \in [50, 450]$W. We verified the accuracy of the look-up table by determining the maximum error in each of its cells. The resulting histogram is shown in Figure 9. Since the error is always bounded above by 0.35%, we conclude that the error introduced by the look-up table is negligible and therefore claim it is not reasonable to replace the look-up table by an online computation of the correction. The exact calculation of a single correction takes approximately 32ms on a standard desktop PC (Intel i5, 2.3Ghz, using a single CPU), for example. Since the pyrometer achieves a sampling rate of 25kHz, this is too slow by about three orders of magnitude. Arguably, the computation time could be reduced with code optimization techniques. From a practical point of view it is, however, desirable to determine the correction on an embedded hardware that is much less powerful than a desktop PC. The evaluation of the look-up table requires 28 summations and 19 multiplications and therefore is ideally suited for online evaluation on an embedded microprocessor.

Finally, we compare the reliability of the pyrometer-based temperature measurement with and without the proposed model-based correction. First note that the temperature recorded with the pyrometer fluctuates by 53K during the calibration run without the correction. With the correction, this figure can be reduced to 18K. In order to carry out an evaluation with data not used for the calibration, we recorded 25960 temperature measurements with the pyrometer for $P = 250$W, $\|U\|_2 = 10$mm/s along a circular path with a diameter of 10mm. The standard deviation of the temperature was reduced from 18.8K without the model-based correction to 8.7K with the proposed model-based correction of the directional dependency. This is illustrated in Figure 10. We stress again this comparison

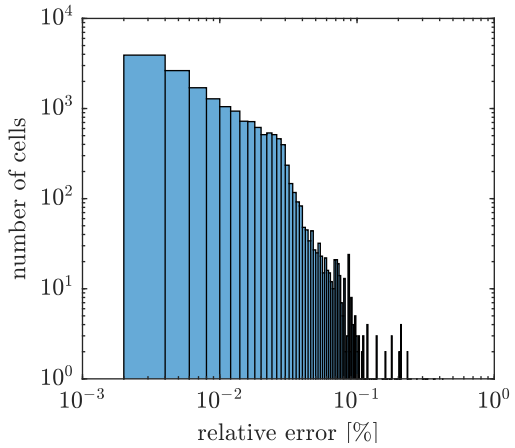

Fig. 9. Histogram of errors introduced by the look-up table. The maximum error that appears amounts to 0.35%.

was carried out after a careful manual minimization of the pyrometer offset. In practical applications, the directional dependence and, thus, the error without a compensation, will in general be larger. In spite of the assumptions that enter the model, specifically the temperature independence of the thermal diffusivity, isotropy and homogeneity, the accuracy of the proposed approach is acceptable.

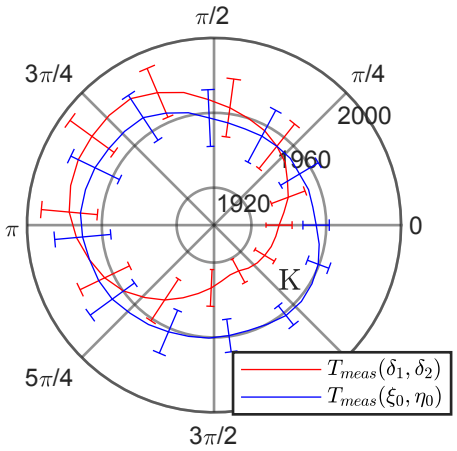

Fig. 10. Comparison of the measurement and the compensated measurement of the pyrometer as a function of the direction $\phi(U)$ (see (1))

5. CONCLUSION

We implemented a method for the model-based correction of temperature measurements in DED processes with point heat sources. We applied the proposed method to a DED laboratory machine and showed the reliability of a pyrometer-based online temperature measurement can be improved considerably.

The present paper focused on the model-based correction of measurements carried out with a misaligned pyrometer. The proposed method is essentially based on determining the pyrometer offset from measured data obtained in a calibration run. Future work will focus on determining the offset online during production runs of the machine. It is an obvious idea to combine such an online estimation with a feedback controller that physically aligns the pyrometer instead of correcting its offset digitally. It remains to investigate whether the physical correction yields results that are superior to those of the digital correction.

ACKNOWLEDGEMENTS

We gratefully acknowledge funding by the German Federal Ministry of Education and Research under grant 13N14305.

REFERENCES

Bai, Y. and Wang, D. (2010). On the comparison of trilinear, cubic spline, and fuzzy interpolation methods in the high-accuracy measurements. *IEEE Transactions on fuzzy Systems*, 18(5), 1016–1022.

Devesse, W., De Baere, D., and Guillaume, P. (2014). Design of a model-based controller with temperature feedback for laser cladding. *Physics Procedia*, 56, 211–219.

Devesse, W., De Baere, D., Hinderdael, M., and Guillaume, P. (2017). Model-based temperature feedback control of laser cladding using high-resolution hyperspectral imaging. *IEEE/ASME Transactions on Mechatronics*, 22(6), 2714–2722.

Dowden, J.M. (2001). *The mathematics of thermal modeling: an introduction to the theory of laser material processing*. Chapman and Hall/CRC.

Gibson, I., Rosen, D., and Stucker, B. (2015). Directed energy deposition processes. In *Additive Manufacturing Technologies*, 245–268. Springer.

Rosenthal, D. (1946). The theory of moving sources of heat and its application of metal treatments. *Transactions of ASME*, 68, 849866.

Song, L. and Mazumder, J. (2010). Feedback control of melt pool temperature during laser cladding process. *IEEE Transactions on control systems technology*, 19(6), 1349–1356.

Wang, Q., Li, J., Gouge, M., Nassar, A.R., Michaleris, P.P., and Reutzel, E.W. (2017). Physics-based multivariable modeling and feedback linearization control of melt-pool geometry and temperature in directed energy deposition. *Journal of Manufacturing Science and Engineering*, 139(2), 021013.

Appendix A. PARAMETERS

Table A.1. Table of physical parameters

Parameter	Symbol	Value
Thermal diffusivity	α	5.006 $10^{-6} m^2/s$
Specific heat	C_p	500 $J/(kgK)$
Thermal conductivity	k	20 $W/(Km)$
Density	ρ	7990 kg/m^3
Melting temperature	T_m	1713.15 K

Table A.2. Table of other parameters

Parameter	Symbol	Value
Maximum measurable temperature	$T_{\max}$	$2573K$
Maximum motion speed	U	20 mm/s
Maximum laser power	$P_{\max}$	$450W$
laser power (for simulations)	P	$250W$
Absorption coefficient	A_b	0.625
Process laser wavelength	λ_L	$1070nm$
Pyrometer wavelength	λ_P	1450-1800nm